Mathematical Models for Tumour Angiogenesis: Numerical Simulations and Nonlinear Wave Solutions

H.M. Byrne and M.A.J. Chaplain
School of Mathematical Sciences,
University of Bath,
Claverton Down,
Bath BA2 7AY, UK.
Telephone: 44 0225 826242
Fax: 0225 826492
e-mail: hmb, majc@uk.ac.bath.maths

Abstract

To ensure its sustained growth, a tumour may secrete chemical compounds which cause neighbouring capillaries to form sprouts which then migrate towards it, furnishing the tumour with an increased supply of nutrients. In this paper a mathematical model is presented which describes the migration of capillary sprouts in response to a chemottractant field set up by a tumour-released angiogenic factor, sometimes termed a tumour angiogenesis factor (TAF). The resulting model admits travelling wave solutions which correspond either to successful neovascularization of the tumour or failure of the tumour to secure a vascular network, and which exhibit many of the characteristic features of angiogenesis. For example, the increasing speed of the vascular front, and the evolution of an increasingly developed vascular network behind the leading capillary tip front (the brush-border effect) are both discernible from the numerical simulations. Through the development and analysis of a simplified caricature model, valuable insight is gained into how the balance between chemotaxis, tip proliferation and tip death affects the tumour's ability to induce a vascular response from neighbouring blood vessels. In particular, it is possible to define the success of angiogenesis in terms of known parameters, thereby providing a potential framework for assessing the viability of tumour neovascularization in terms of measurable quantities.

1 Introduction

Unless furnished with an adequate blood supply and a means of disposing of waste products by a mechanism other than diffusion, a solid tumour cannot grow beyond a few millimetres in diameter and remains in an *avascular* state. Avascular nodules can be cultivated in the laboratory (Folkman, 1976) or can be found *in vivo* (carcinomas *in situ* being a good example) and typically consist of a central necrotic core surrounded by a thin outer layer of live, proliferating cells. Mathematical models describing this avascular growth can be found in, for example, Greenspan (1976), Chaplain (1990), Adam and Maggelakis (1990), and references therein.

Transition from this dormant avascular state to the vascular state, wherein the tumour possesses the ability to invade surrounding tissue and metastasise to distant parts of the body, depends upon its ability to induce new blood vessels from the surrounding tissue to sprout towards and then gradually penetrate the tumour, thus providing it with an adequate blood supply and microcirculation. In order to accomplish this *neovascularization*, it is now a well-established fact that tumours secrete a number of diffusible chemical compounds into the surrounding tissue and extracellular matrix. Much work has been carried out into the nature of such factors and their effect on endothelial cells since initial research began in the early 1970's with Folkman, culminating in the purification of several tumour angiogenic factors, the cloning of their genes from libraries of complementary DNA (cDNA) and the determination of their amino acid sequences (Strydom *et al.,* 1985; Folkman and Klagsbrun, 1987; Deshpande and Shetna, 1989). Throughout the rest of this paper, we use TAF as a generic term for the various growth factors and other chemicals which elicit a response from neighbouring blood vessels. The extensive literature on the subject is testimony to its importance in our understanding of the mechanisms by which solid tumours develop and grow (see, for example, the reviews of Folkman and Klagsbrun, 1987, and Paweletz and Knierim, 1989). Various experimental techniques and model systems have been developed in order to study and identify the processes involved in angiogenesis and these include implanting a section or fragment of a solid tumour into the cornea of various test animals such as the rabbit (Gimbrone *et al.*, 1974) or mouse (Muthukkaruppan *et al.*, 1982), the dorsal air sac in the rat (Folkman, 1976), the hamster cheek pouch chamber (Eddy and Casarett, 1973), the chick embryo chorioallantoic membrane (CAM) (Ausprunk *et al.*, 1974; Klagsbrun *et al.*, 1976; Ishiwata *et al.*, 1988) and capillary endothelial cells in tissue culture (Jaffe *et al.*, 1973; Birdwell *et al.*, 1977; Madri and Pratt, 1986). These model systems enable us to document the complete sequence of events which takes place during tumour-related angiogenesis.

In response to the angiogenic stimulus, or TAF, which has been secreted into the surrounding host tissue by the tumour cells, the endothelial cells of neighbouring capillaries firstly release proteolytic and collagenolytic enzymes that degrade and disintegrate their basal lamina and the intercellular matrix through which they must move. They then migrate towards the solid tumour, the source of the angiogenic stimulus. Solid sprouts are formed as the endothelial cells elongate and align with one another. The proliferation of endothelial cells a short distance behind the sprout tip contributes to the number of migrating cells. Thus solid strands of endothelial cells are formed in the extracellular matrix, lumina develop within these strands, and mitosis continues, increasing the sprout length. Anastomosis – the process whereby reconnections and fusions form a closed network – occurs between neighbouring sprouts, with the formation of loops which network the blood circulation. Pericytes appear at the base of the loops and the endothelial cells form a basal lamina. New sprouts can now grow from the loops, thus continuing the angiogenic process, in a self-similar fashion, until the capillary sprouts finally penetrate the tumour, and neovascularization takes place. During this vascular phase of growth, invasion of the surrounding tissue by tumour cells and metastasis is anticipated. A comprehensive description of the above events can be found in the extensive review of Paweletz and

Knierim (1989).

Although angiogenesis may appear to be a particularly insidious facet of tumour growth, this apparent strength has been exploited in order to control, or even stop altogether, any subsequent growth by developing an *anti-angiogenesis* strategy (Folkman, 1974). Drugs have been sought which prevent the formation of new capillary growth (Langer *et al.*, 1980; Gross *et al.*, 1981). Indeed the clear differences between normal blood vessels and those present in neovascularized tumours (Kumar *et al.*, 1985; Erroi *et al.*, 1986) are now being exploited to develop drugs which can recognise and distinguish between normal tissue and the solid tumour. This specific targetting of the tumour itself offers great potential for patient chemotherapy (Willmott *et al.*, 1991).

The aim of this paper is to examine mathematical models of angiogenesis, formulated in terms of continuous variables, which yield qualitative phenomenological results. In particular, we focus on the model of Balding and McElwain (1985) which was developed from a fungal growth model proposed by Edelstein (1982). Modelling of this nature can predict the behaviour of certain averaged quantities such as vessel and tip densities per volume tissue, but is unable to provide the details of microscopic features, such as vessel lengths and distances between buds or anastomoses, that can be obtained using stochastic modelling approaches (Stokes and Lauffenburger, 1991). One improvement arising from the modelling approach adopted in this paper is the ability to predict the brush-border effect of the advancing vascular front which has been observed experimentally by Muthukkaruppan *et al.* (1982), and which neither Balding and McElwain's nor Stokes and Lauffenburger's models were able to predict. The brush-border effect describes the evolution of an increasingly developed vascular network behind the leading tip front, with the tip density attaining a maximum value ahead of the vessel density.

In the next section we describe our modified version of the Balding and McElwain model (1985), indicating how and why the model has been adapted. The resulting numerical simulations are then presented in section 3 where they are compared with those of Balding and McElwain. Section 4 continues with the development of a simplified model which describes the propagation of the vascular front towards the tumour, after the TAF concentration profile has reached a steady-state and the initial formation of capillary sprouts has been successfully accomplished. The resulting model enables us to focus on how the balance between sprout tip proliferation, tip death, and the strength of the chemotactic gradient dictate the outcome of the neovascularization process. In particular, by constructing upper and lower bounds for the tip density, regions of parameter space are identified in which neovascularization succeeds or fails. (In the case of successful neovascularization, a new model is needed to describe the final stages of the process, as the tips penetrate the tumour.) Thus the model provides a framework for assessing the viability of tumour neovascularization in terms of specific, measurable parameters and for developing anti-angiogenesis strategies.

2 The Mathematical Model

In this section and throughout the rest of the paper we choose to focus on the model system of Gimbrone *et al.* (1974) and Muthukkaruppan *et al.* (1982) wherein a fragment of tumour is implanted into the cornea of a test animal and an angiogenic response is elicited from blood vessels situated in the nearby limbus region of the cornea. Once an underlying chemottractant field has been established, the process of tumour-induced capillary growth takes place in three distinct stages:

- Secretion of enzymes by the endothelial cells causes degradation of the basal lamina and leads to the formation of capillary buds or sprouts;
- Migration of the sprouts towards the tumour;
- Contact between the capillaries and the tumour.

By focussing, in this paper, on the second phase of the neovascularization process, we describe the motion of the capillary sprouts in response to the underlying TAF field, illustrating, where possible, whether neovascularization will occur. For example, we shall show in section 4 that the chemottractant field may not be strong enough to successfully vascularise the tumour. Accurate descriptions of the initial and final stages of neovascularization call for different modelling approaches not considered here. We focus on the second stage as being the rate-limiting stage in the angiogenesis process.

Following Balding and McElwain (1985), the continuum model of tumour-induced capillary growth which we propose is based on the fungal growth model of Edelstein (1982), the two processes sharing many common features, for example branching, anastomosis and migration.

Now, angiogenesis is essentially a multidimensional process with new tips sprouting in directions other that that of the advancing front. By averaging the dependent variables in a plane perpendicular to the direction of motion of the vascular front, it is possible to restrict attention to one spatial dimension, in the direction of the line connecting the tumour fragment to the nearest limbal vessels. Thus, we introduce independent variables t and x with t representing time and the x-axis lying parallel to the direction of tip growth, such that the tumour lies at $x = 0$ and the limbus at $x = L$. Three averaged dependent variables are used to describe the relevant physical processes: sprout tip density n which we interpret as the number of tips per unit cross-sectional area in the plane perpendicular to the direction of front propagation; vessel density ρ which we interpret as the vascular content per unit cross-sectional area; and, the chemoattractant (TAF) concentration c which we interpret as the mean concentration per unit cross-sectional area. Thus, no distinction is made between primary and secondary vessels, or between new and old vessels. Similarly, only a single, composite or generic TAF is considered – experimental results suggest that a number of angiogenic factors may be secreted by a tumour, each with its own chemical properties. The above assumptions are adopted in order to minimise the complexity of the model.

Again following Balding and McElwain, it is assumed that the capillary density can increase only by the movement of the sprout tips and that vessel decay is a first order process. Thus, we propose that

$$\frac{\partial \rho}{\partial t} = -nv - d, \tag{1}$$

where $v(x,t)$ is the velocity of the tips, specified below, and d is the death rate of capillaries, in units of capillary length per unit area per unit time. Since capillaries regress when the source of TAF is removed, it is also assumed that vascular decay is a feature of tumour induced angiogenesis and that a fixed proportion γ_1 of branches are broken down in each time unit, giving

$$d = \gamma_1 \rho.$$

Applying conservation of mass, the equation for tip density $n(x,t)$ is given as

$$\frac{\partial n}{\partial t} = -\frac{\partial J}{\partial x} + \sigma, \tag{2}$$

where $J(x,t)$ is the tip density flux, and σ is the net tip creation rate. Evidence that the tip extension speed v is related to a chemotactic response of endothelial cells is accounted for by assuming that J consists of two terms, one due to random motion, the other due to chemotaxis in the presence of the TAF. Denoting by μ_1 and χ_1 the assumed constant motility and chemotactic coefficients, the flux of tips is given by

$$\begin{aligned} J(x,t) &= J_{\text{random}} + J_{\text{chemotactic}} \\ &= -\mu_1 \frac{\partial n}{\partial x} + \chi_1 n \frac{\partial c}{\partial x}. \end{aligned} \tag{3}$$

Whilst Balding and McElwain argue that, since sprouts are never observed directed away from the tumour, random motion is negligible, and, hence, $\mu_1 = 0$, more recent models by Stokes and Lauffenburger (1991), Chaplain and Stuart (1991,1993), and experimental evidence by Paweletz and Knierim (1989) seems to indicate otherwise. Simulations by Stokes and Lauffenburger demonstrate that the inclusion of a directionally random motility factor at the sprout tip is required for vessel anastomosis and capillary loop formation whilst Paweletz and Knierim describe the path of the sprouts towards the tumour as one of least resistance. Thus the sprouts use collagen fibres or fibrin strands as guidelines for their growth. Although this is not, in essence, random motion, it can be modelled as such. It seems therefore reasonable to retain the motility coefficient μ_1.

Equating J with nv leads to the following equation for the tip extension rate

$$v = -\mu_1 \frac{1}{n}\frac{\partial n}{\partial x} + \chi_1 \frac{\partial c}{\partial x}.$$

In (2) the net tip creation rate σ is a balance between tip creation σ_C and tip annihilation σ_A, in units of tips per unit area per unit time (Edelstein, 1982). Experimental results by Gimbrone *et al.* (1974) and Muthukkaruppan *et al.* (1982) suggest that two mechanisms contribute to the tip proliferation rate. Directly after tumour implantation, tip proliferation arises from secondary branching behind the leading tip density front, with tips emanating from the capillary vessels, and stimulated by the presence of TAF. Denoting by α_0 the rate of appearance of tips per unit area per unit TAF concentration for a unit length of branch per unit area (Edelstein, 1982), the following contribution to σ_C is proposed to describe this first mechanism

$$\alpha_0 c \rho.$$

Once the migrating vasculature has advanced further towards the tumour, tip proliferation at the leading vascular edge multiplies rapidly. Supported by experimental results (Chaplain and Stuart, 1991, 1993; Paweletz and Knierim, 1989), we postulate the existence of a threshhold TAF concentration $\hat{c}$ which triggers this secondary type of tip proliferation when $c > \hat{c}$. Assuming further that this rate is proportional to the TAF concentration and the tip density, its contribution to σ_C is given by

$$\alpha_1 H(c - \hat{c}) n c,$$

where α_1 is the rate of secondary tip proliferation, per unit TAF concentration, per tip, when the TAF concentration is sufficiently large, and $H(.)$ is the Heaviside step-function ($H(x) = 1$ if $x > 0$, $H(x) = 0$ if $x \leq 0$). Given that a number of angiogenic factors may be secreted by the tumour (Strydom *et al.*, 1985; Folkman and Klagsbrun, 1987; Deshpande and Shetna, 1989), the two proliferation rates proposed above may be attributed to two distinct factors with different chemical characteristics.

Tip annihilation due to anastomosis is necessary to create an interconnected network of vessels and must be predominant in regions of high capillary density, to prevent unnecessary growth. Whilst tip-to-tip interactions are possible, to minimise the complexity of the model, here attention is restricted to tip-to-branch anastomosis and the following tip annihilation rate proposed

$$\sigma_A = -\beta_2 \rho n,$$

where β_2 is a constant.

To complete the model, an expression for $c(x, t)$ is needed. We assume that the TAF concentration is governed by a reaction-diffusion equation, with first-order decay in the absence of capillary tips. Following Chaplain and Stuart (1991, 1993), and Ausprunk and Folkman (1977), a second sink term describing TAF consumption due to tip proliferation is incorporated, and assumed to take the same form as the secondary tip proliferation rate described above. Thus we propose

$$\frac{\partial c}{\partial t} = D\frac{\partial^2 c}{\partial x^2} - \lambda_1 c - \alpha_1 H(c-\hat{c})nc, \tag{4}$$

where D is the (assumed constant) diffusion coefficient of TAF in the cornea, and λ_1 its natural decay rate, so that Balding and McElwain's limit is recovered by setting $\lambda_1 = 0 = \alpha_1$. The absence in (4) of a specific source term reflects the fact that TAF is only produced by the tumour cells, which remain at $x = 0$: TAF production is incorporated via the boundary condition imposed at $x = 0$ where a constant concentration c_0 is maintained (see equations (7)).

In order to close the system defined by (1)–(4), appropriate boundary and initial conditions are imposed. At the tumour, the TAF concentration is maintained at the constant value c_0, and the tip density is set to zero, so that our model no longer applies when the tips have penetrated the tumour. At the limbus, the TAF concentration is set to zero whilst the tip and vessel densities decay exponentially to zero and ρ_{min} respectively, at the rate k s^{-1}. The latter conditions are motivated by experimental results which suggest that, after the initial formation of capillary buds at the limbus, sprout tips no longer originate from the limbus – there is one-off formation of sprout tips at $x = L$ at $t = 0$. Continual recruitment of endothelial cells from the parent vessel motivates the decay to ρ_{min} of the vessel density at the limbus (Paweletz and Knierim, 1989; Stokes and Lauffenburger, 1991). As the tips propagate towards the tumour, a network of vessels forms behind them and, therefore, if the advancing front is to maintain contact with the limbus, the vessel density at the limbus must not fall below some value, ρ_{min} say. Initial TAF, tip and vessel densities, consistent with the boundary conditions, are prescribed. In summary, the following boundary and initial conditions are imposed.

$$\rho(L,t) = \rho_{min} + (\rho_L - \rho_{min})e^{-kt},\ \rho(x,0) = 0 \text{ for } 0 \le x < L,\ \rho(L,0) = \rho_L, \tag{5}$$

$$n(0,t) = 0,\ n(L,t) = n_L e^{-kt},\ n(x,0) = 0 \text{ for } 0 \le x < L,\ n(L,0) = n_L, \tag{6}$$

$$c(0,t) = c_0, c(L,t) = 0, c(x,0) = c_0(x) \text{ for } 0 < x \leq L, \tag{7}$$

where ρ_L, n_L and c_0 are characteristic values for ρ, n and c at the limbus and tumour, respectively.

Nondimensionalisation

Before continuing it is helpful to recast the model in dimensionless variables, rescaling distance with the limbus-tumour distance L, and time with $\tau = L^2/D$ which is the time for TAF to diffuse from the tumour to the limbus. The dependent variables and key parameters are rescaled thus:

$$\rho^* = \rho/\rho_L,\ n^* = n/n_0,\ n_L^* = n_L/n_0,\ c^* = c/c_0,\ \hat{c}^* = \hat{c}/c_0,$$
$$\rho_{min}^* = \rho_{min}/\rho_L,\ k^* = k/\tau,\ \mu^* = \mu_1/D,\ \chi^* = \chi_1 c_0/D,\ \gamma^* = \gamma_1\tau,$$
$$\alpha_0^* = \alpha_0 c_0 L\tau,\ \alpha_1^* = \alpha_1\tau c_0,\ \beta^* = \beta_2\tau\rho_L,\ \lambda^* = \lambda_1\tau.$$

Dropping the asterisks, and substituting for v and $\sigma = \sigma_C - \sigma_A$, the governing equations transform to give

$$\frac{\partial \rho}{\partial t} = \mu\frac{\partial n}{\partial x} - \chi n\frac{\partial c}{\partial x} - \gamma\rho, \tag{8}$$
$$\frac{\partial n}{\partial t} = \mu\frac{\partial^2 n}{\partial x^2} - \chi\frac{\partial}{\partial x}\left(n\frac{\partial c}{\partial x}\right) + \alpha_0\rho c + \alpha_1 H(c-\hat{c})nc - \beta n\rho, \tag{9}$$
$$\frac{\partial c}{\partial t} = \frac{\partial^2 c}{\partial x^2} - \lambda c - \alpha_1 H(c-\hat{c})nc, \tag{10}$$

subject to

$$\rho(1,t) = \rho_{min} + (1-\rho_{min})e^{-kt},\ \rho(x,0) = 0 \text{ for } 0 \leq x < 1,\ \rho(1,0) = 1, \tag{11}$$
$$n(0,t) = 0,\ n(1,t) = n_L e^{-kt},\ n(x,0) = 0 \text{ for } 0 \leq x < 1,\ n(1,0) = n_L, \tag{12}$$
$$c(0,t) = 1, c(1,t) = 0, c(x,0) = 0 \text{ for } 0 < x \leq 1. \tag{13}$$

Estimation of Parameters

Before proceeding with numerical simulations of the system proposed above in equation (8)–(13), estimates of those parameters which can can be determined from the literature are presented. The absence of suitable experiments forces us to use numerical simulations to obtain estimates of the remaining parameters, γ, $\alpha_0, \alpha_1, \lambda, n_L$ and k, judging that appropriate values have been obtained when there is good qualitative agreement between the numerical and experimental results.

From data supplied by Folkman (1976), we adopt 14 days as the average time for vascularisation to occur. For the numerical simulations we define the (dimensionless) time of vascularisation as the earliest time at which a nonzero tip density is recorded at the tumour, and, from these simulations, we observe that this time is largely independent of the system parameters, $\equiv 4$ dimensionless time units. Recalling that the diffusion timescale $\tau = L^2/D$ was used to nondimensionalise the model, we now equate Folkman's experimental with our numerical results to obtain an estimate of $\tau \sim 3.5$ days. Assuming a tumour-limbus separation of 3 mm then leads to an estimate for the TAF coefficient of $D \sim 10^{-8}$ cm^{2}s^{-1}.

Experiments by Rupnick *et al.* (1988) and Stokes *et al.* (1990), Stokes *et al.* (1991) which involved stimulating the movement of endothelial cells in different gradients of angiogenic factors, furnish us with estimates of χ and β. Measuring the chemotactic response of angiogenic factors in concentrations of acidic fibroblast growth factors of approximately 10^{-10}M, they obtained estimates of $\chi_1 = 2.6 \times 10^3$ cm^2 s^{-1}M^{-1}, which correspond to estimates of $\chi = 2.6$ (assuming a diffusion constant $D \sim 10^{-8}$ cm^2 s^{-1}). Further, a value of 0.4 hr^{-1} for the redistribution rate of cells was employed, which here can be equated to the constant β_2, leading to an estimate of $\beta = 45$ (assuming $\rho_L \sim 0.3$ and recalling that $\tau \sim 14$ days). The parameter values used by Stokes and Lauffenburger describe endothelial cell movement in human tissue whereas those used by Balding and McElwain describe angiogenesis in the cornea. Since the cornea is more resistive to endothelial cell movement than normal tissue, we expect that a smaller value of χ would be appropriate and we, therefore, conclude that Balding and McElwain's choice of $\chi = 1$ for the cornea is reasonable.

Turning now to the motility ratio μ, Rupnick *et al.* (1988) and Stokes *et al.* (1990) obtained estimates for the random motility of individual microvessel endothelial cells in isolated systems. Their experiments gave rise to values of $\mu_1 = D/\mu$ in the range 2×10^{-9} to 10^{-8} cm^2 s^{-1}. With $D \sim 10^{-8}$ cm^2 s^{-1}, these yield dimensionless estimates of μ in the range 0.2 to 1. However, our model focuses on the motion of the capillary sprout tips rather than individual endothelial cells and we do not make the assumption that the motion of a capillary sprout tip is determined by a single endothelial cell. The results of Rupnick *et al.* (1988) demonstrate that when the movement of individual endothelial cells is constrained by surrounding cells the agreement between their theory and experiment is poor. The morphological data of Paku and Paweletz (1991) show that from a very early stage and subsequently throughout angiogenesis, the EC remain in contact, via junctions, with the EC of the parent vessel. It is also known that during angiogenesis the growing capillaries follow the path of least resistance during their motion (Paweletz and Knierim, 1989). Indeed once the capillary network is established the capillary sprouts form blind-end tubes with the end of sprout tip being hollow (Paweletz and Knierim, 1989). Finally we note that the results of Stokes and Lauffenburger (1991) demonstrate that angiogenesis simulated with random motility only (i.e. no chemotaxis) produces very poor results which do not agree at all with the capillary networks observed *in vivo.* We conclude that chemotaxis is the dominant effect and that the value chosen for μ should reflect this and hence we fix $\mu = 10^{-3}$ which corresponds to a dimensional value of $\mu_1 = 10^{-11}$ cm^2 s^{-1}. As the numerical simulations presented in section 3 show, this value gives rise to tip and vessel densities which are in good qualitative agreement with the experimental results (Gimbrone *et al.*, 1974; Muthukkaruppan *et al.*, 1982; Paweletz and Knierim, 1989). Simulations performed with larger values of μ, for example $\mu \sim 10^{-2}$, yielded similar qualitative results, albeit at a more rapid rate, and with much of the fine structure smoothed out.

Henceforth we fix $(\chi, \beta, \mu) = (1.0, 35, 10^{-3})$, and base our estimates of the remaining parameters, $(\gamma, \alpha_0, \alpha_1, \lambda, k, n_l)$, on the numerical simulations presented in the next section.

3 Numerical Results

The system of partial differential equations (8)–(10), subject to the boundary and initial conditions (11)–(13), were solved using the Method of Lines and Gear's Method, as implemented by the NAG Fortran Library routine DO3PGF.

Figures 1(a,b,c) shows the profiles of the capillary tip density, the vessel density, and the TAF concentration in the external host tissue at regular time intervals when successful angiogenesis occurs. As has been mentioned earlier, the solution remains valid while the vascular front is crossing the tissue space and has not yet reached the tumour. From figure 1(a) we observe that this condition holds until $t = 1.6$, at which time n is nonzero in a neighbourhood of $x = 0$ and the model is no longer valid since interactions between tumour cells and the vasculature become important. The time taken for the tips to first reach the tumour corresponds to a real time of approximately 20 days, which is within Balding and McElwain's experimentally determined timescale (see Balding and McElwain, 1985, and references therein). By varying the system's parameters the time taken for the capillary sprouts to reach the tumour can be varied. The sharp transition in the branch density and, to a lesser extent, the tip density observed at $x \sim 0.8$ in figures 1(b,a) is caused by the initiation of secondary tip proliferation there. From figure 1(c) we see that $c(x,t) < \hat{c} = 0.2$ for $x \in (0.8, 1)$ and that $c(x,t) > \hat{c}$ for $x \in (0, 0.8)$. Further, we observe the the maximum tip density is located behind the leading front, increases in magnitude as the front develops, and precedes the maximum vessel density. Thus, the qualitative features of the brush-border effect observed by Muthukkaruppan *et al.* (1982) are reproduced. Inspection of figures 1(a,b) also shows that the speed of propagation of the vascular front increases as the tumour is approached, a result consistent with experimental measurements by Folkman (1986).

Figures 2(a,b,c) show the profiles for (n, ρ, c) for a TAF field which, compared with figures 1(a,b,c), decays more rapidly and elicits a weaker secondary tip proliferation response. In particular, the parameters $\hat{c}$ and λ are increased to $\hat{c} = 0.5$ and $\lambda = 10.0$. The resulting vascular response is very weak, indicating that the underlying TAF field plays a major role in establishing tumour neovascularization.

Figures 3(a,b,c), which show the profiles for (n, ρ, c) when no secondary tip proliferation occurs ($\alpha_1 = 0$), are included for comparison with Balding and McElwain's simulations. Working on an infinite domain, with no secondary tip proliferation, their simulations show the tip and vessel density maxima occurring simultaneously. Given that in figures 3(a,b) the maximum tip density still precedes the maximum vessel density, we conclude that posing the model on a finite domain is instrumental in reproducing the tip/vessel-density lag-effect. In addition, given that the tip density profiles in figure 1(a) are more pronounced than those in figure 3(a), we deduce that the secondary proliferation rate is instrumental in reproducing the brush-border effect (Muthukkaruppan *et al.*, 1982).

Comparing figures 1(c), 2(c) and 3(c) we observe that for each simulation the TAF rapidly attains a steady profile which is monotonically decreasing in x. This will be exploited in the next section where a simplified model for tumour angiogenesis is developed.

4 Model Simplification and Mathematical Analysis

In this section we develop a simplified version of the TAF model which provides insight into how the balance between chemotaxis, tip proliferation, and tip death affects the ability of a tumour to induce a vascular response from the neighbouring limbus.

The numerically-computed profiles obtained by both Balding and McElwain and in section 3 indicate that, when successful neovascularization occurs, the leading edge of the tip density profile, which marks the extent of tip penetration into the tissue, advances towards the tumour. Further, the maximum tip density is located behind the leading front and increases in magnitude as the front develops. Balding and McElwain's simulations show the peak tip and vessel densities occurring simultaneously whereas our numerical results resolve these maxima, the tip density maximum preceding that of the vessels. The latter results are consistent with observations by Muthukkaruppan *et al.* (1982) of the brush-border effect.

Working on a semi-infinite spatial domain, with $\lambda = 0 = \alpha_1$ in (10), Balding and McElwain described the underlying TAF field in terms of error functions, which are fundamental solutions of the diffusion equation. However, our numerical results suggest that, when posed on a finite domain, the underlying TAF concentration relaxes rapidly to a steady profile which is monotonic decreasing with respect to x. For example, fixing $\alpha_1 = 0$ in (10) we obtain the following steady-state TAF profile

$$c(x) = \frac{\sinh \sqrt{\lambda}(1-x)}{\sinh \sqrt{\lambda}}. \tag{14}$$

Noting the definition of the dimensionless parameter λ, we remark that, as a result of the nondimensionalisation process, even though our model is posed on the unit interval, it is possible to simulate an increased domain size by increasing λ (and changing other parameters accordingly). This has the effect of reducing the gradient

$\dfrac{dc}{dx}$ near the limbus and hence reducing the chemotactic response . Addition of an anti-angiogenic factor, and inherent resistance of the tissue to penetration by TAF, effect similar changes in λ and the chemotactic response as that induced by increasing the tumour-limbus separation. Thus we believe that the finite domain approach adopted here not only provides greater flexibility for simulating different experimental configurations but it is also closer to the underlying setup than the semi-infinite domain approach.

Recalling the estimate of $\mu \sim 10^{-3}$, and now following Balding and McElwain, we henceforth neglect tip motility and fix $\mu = 0$ in (8), (9). Adopting the steady TAF approximation, with $c(x,t) \equiv c(x)$ defined by (14), equations (8)–(13) reduce to give

$$\frac{\partial \rho}{\partial t} = -\chi n \frac{dc}{dx} - \gamma \rho, \tag{15}$$

$$\frac{\partial n}{\partial t} = -\chi \frac{\partial}{\partial x}\left(n \frac{dc}{dx}\right) + \alpha_0 \rho c + \alpha_1 n c H(c - \hat{c}) - \beta n \rho, \tag{16}$$

subject to

$$\rho(x,0) = 0 \text{ for } x \in [0,1),\ \rho(1,0) = 1, \tag{17}$$

$$n(0,t) = 0,\ n(x,0) = n_0(x) \text{ for } x \in [0,1],\ n(1,t) = n_L. \tag{18}$$

Since the simplified model, proposed here, assumes that the TAF concentration has reached its steady-state configuration, it is reasonable to assume that any transients associated with initiating propagation of the vascular front have also decayed away. The starting point for this caricature model corresponds then to a situation in which new tips occupy a finite neighbourhood of the limbus, $(x^*, 1)$ say. Hence, we prescribe

$$n(x,0) = n_0(x) = \begin{cases} 0 & x \in [0, x^*), \\ 1 & x \in [x^*, 1], \end{cases}$$

with $n(1,t) = n_L = 1$, for consistency.

One approach to the analysis of (15)–(18) is a "classical" travelling wave analysis, valid in the limit when the tip proliferation and tip death rate constants satisfy $(\alpha_0, \alpha_1, \beta) \sim O(\delta^{-1})$, for some small parameter δ (Berestycki *et al.*, 1983; Fife, 1979). (From the numerical simulations, we anticipate $\delta \sim O(10^{-2})$.) In this case, the trivial outer solutions, which correspond to avascular ($n = 0 = \rho$) and vascular ($n, \rho > 0$) states are connected by a proliferating region, or boundary layer, of width δ, in which tips and branches are produced. This production zone propagates with speed $\sigma \sim O(\delta)$ through the tissue towards the tumour. Such an approach entails posing the problem on the infinite domain, which runs counter to the prevailing approach outlined above, and is, therefore, not considered further.

The approach adopted here describes a quasi-steady situation for which the vessels respond instantaneously to changes in the tip density, so that $\dfrac{\partial}{\partial t} = 0$ in (15). Whilst this limit may be somewhat artificial, we believe that it is of interest in extending our understanding of the balance between the competing physical effects which occur in angiogenesis. Further, the resulting tip and vessel density profiles exhibit the same qualitative features as their numerically-simulated counterparts, the latter obtained from the full model. Additional results which characterise the success or failure of angiogenesis in terms of known parameters justify, a posteori, the adoption of the quasi-steady approach in preference to the classical travelling wave discussed outlined above.

With $c(x)$ defined by (14), and making the quasi-steady approximation $\dfrac{\partial}{\partial t} = 0$ in (15), we deduce that the vessel density can be expressed in terms of the tip density as follows

$$\rho(x,t) = -\frac{\chi}{\gamma}\frac{dc}{dx}n = \left(\frac{\chi\sqrt{\lambda}\cosh\sqrt{\lambda}(1-x)}{\gamma\sinh\sqrt{\lambda}}\right)n(x,t).$$

Thus, the vessel density is bounded by a multiple of the tip density. Substitution with $c(x)$ and $\rho(x,t)$ in (16) yields the following nonlinear wave equation which defines $n(x,t)$:

$$\frac{\partial n}{\partial t}+\chi\frac{dc}{dx}\frac{\partial n}{\partial x}=\left\{\alpha_1 H(c-\hat{c})-\chi\lambda-\frac{\alpha_0\chi}{\gamma}\frac{dc}{dx}\right\}cn+\frac{\beta\chi}{\gamma}\frac{dc}{dx}n^2\equiv F(n,c), \qquad (19)$$

subject to (18). From (19) we note that the wavespeed is given by

$$\frac{dx}{dt}=\chi\frac{dc}{dx}=-\frac{\chi\sqrt{\lambda}\cosh\sqrt{\lambda}(1-x)}{\sinh\sqrt{\lambda}}$$

so that, as anticipated, the wave propagates from the limbus ($x=1$), with increasing speed, to the tumour ($x=0$). This result is qualitatively consistent with the numerical simulations of section 3 and experimental measurements which show tip velocities increasing from 0.2mm s^{-1} to 0.8 mm s^{-1} as the vascular front approaches the tumour (Folkman, 1986).

Using the method of characteristics (Williams, 1980), it is possible to construct explicit solutions of (19), subject to (18). As mentioned in section 2, the final stages of angiogenesis, when contact is made between the capillaries and the tumour, are not addressed here. Thus we expect our model to remain valid only whilst $n(0,t)=0$: given the compact support of the initial data, that is until those tips initially located at $x=x^*$ reach $x=0$ (specifically, for the case $0<\lambda\ll 1$, discussed below, until $t=x^*/\chi$).

Using independent variables $(s,r)=(s(x,t),r(x,t))$ to parameterise arc-length along a characteristic and initial data respectively, we deduce from (19) that n satisfies

$$\frac{\partial n}{\partial s}\equiv\frac{\partial n}{\partial t}+\chi\frac{dc}{dx}\frac{\partial n}{\partial x}=F(n,c). \qquad (20)$$

Recalling that $\rho=-\dfrac{\chi}{\gamma}\dfrac{dc}{dx}n$, we deduce further that along a characteristic

$$\frac{\partial \rho}{\partial s}=\frac{\partial \rho}{\partial t}+\chi\frac{dc}{dx}=-\frac{\chi}{\gamma}\frac{dc}{dx}\left(\frac{\partial n}{\partial s}+\chi n\frac{d^2c}{dx^2}\right). \qquad (21)$$

Now, with c given by (14), at a stationary point for the tip density

$$\frac{\partial n}{\partial s} = 0 \Rightarrow \frac{\partial \rho}{\partial s} = -\frac{\chi^2}{\gamma}\frac{dc}{dx}\frac{d^2c}{dx^2}n > 0,$$

so that the vessel density is still increasing there. Similarly,

$$\frac{\partial \rho}{\partial s} = 0 \Rightarrow \frac{\partial n}{\partial s} = -\chi n \frac{d^2c}{dx^2} < 0,$$

so that where n attains its maximum value ρ is still increasing and where ρ attains its maximum n is decreasing. Now, for a fixed value of x, s may be regarded as a timelike variable and the above result interpreted as follows. When the tip density attains its maximum value at a given point between the tumour and the limbus, the vessel density there is still increasing. Conversely, when the vessel density attains its maximum at the same point in space, the tip density is decreasing there. Thus, the simplified model retains the qualitative features of the numerical simulations presented in section three: as the vascular front advances toward the tumour the maximum tip density precedes the maximum vessel density, a result consistent with the experimental observations of Muthukkaruppan *et al.* (1982).

To simplify the analysis, we assume that $0 < \lambda \ll 1$, in which case, to leading order in λ, the steady TAF profile satisfies

$$c(x) = 1 - x,$$

the vessel density is directly proportional to the tip density ($\rho = \chi n/\gamma$), and equation (19) reduces to give

$$\frac{\partial n}{\partial t} - \chi\frac{\partial n}{\partial x} = \left(\alpha_1 H(1 - x - \hat{c}) + \frac{\alpha_0 \chi}{\gamma}\right)(1 - x)n - \frac{\beta\chi}{\gamma}n^2 + O(\lambda). \qquad (22)$$

Since secondary tip proliferation is active only when $x \in (0, 1 - \hat{c})$ and the characteristics of (22) are the family of straight lines $x + \chi t = \text{constant}$, we remark that (x, t)-space may be partitioned into distinct regions according to the influence of the initial data and whether secondary tip proliferation occurs there. Integrating along characteristics in the regions defined in figure 4, the following expressions for the tip density may be obtained:

$$n_0(x,t) \equiv 0,$$

$$n_1(x,t) = \frac{\exp\{\frac{\alpha_0\chi}{\gamma}t(1-x-\chi t/2)\}}{1+\frac{\beta\chi}{\gamma}\int_0^t \exp\{\frac{\alpha_0\chi}{\gamma}\tau(1-x-\chi t+\chi\tau/2)\}d\tau},$$

$$n_2(x,t) = \frac{n_1(1-\hat{c},t-(1-\hat{c}-x)/\chi)\exp\{(\frac{\alpha_0\chi}{\gamma}+\alpha_1)(1-\hat{c}-x)(1+\hat{c}-x)/2\chi\}}{1+\frac{\beta\chi}{\gamma}n_1(1-\hat{c},t-(1-\hat{c}-x)/\chi)\int_0^{(1-\hat{c}-x)/\chi}\exp\{(\frac{\alpha_0\chi}{\gamma}+\alpha_1)\eta(\hat{c}+\chi\eta/2)\}d\eta},$$

with similar expressions holding in regions 3 and 4, and the solution remaining valid until $t = x^*/\chi$, at which time the characteristic passing through $(x,t) = (x^*,0)$ reaches the tumour.

From the partial differential equation governing the tip density it is clear that success, or failure, of angiogenesis depends on the balance between tip proliferation, tip decay, and the speed of propagation of the vascular front, the latter dictated by the strength of the chemotaxis gradient. In order to gain more precise information into how these competing effects interact, we now derive upper and lower bounds for the tip density at $(0, x^*/\chi)$ for the case $\alpha_0 = 0$, so that secondary tip proliferation is the dominant mechanism for tip production. Given that the initial tip density is normalised to unity, these bounds may be used to determine criteria under which angiogenesis succeeds (the lower bound exceeds unity) and under which angiogenesis fails (the upper bound is less than unity). Using the above expressions, with $\alpha_0 = 0$, we deduce

$$n_2(0,x^*/\chi) = \frac{n_1(1-\hat{c},T)e^\theta}{1+\frac{\beta\chi}{\gamma}n_1(1-\hat{c},T)\int_0^{(1-\hat{c})/\chi}\exp\{\alpha_1\eta(\hat{c}+\chi\eta/2)\}d\eta}, \tag{23}$$

where we have introduced $T = [x^* - (1-\hat{c})]/\chi$ and $\theta = \alpha_1(1-\hat{c}^2)/2\chi$, and

$$n_1(1-\hat{c},T) = (1+\frac{\beta\chi T}{\gamma})^{-1}.$$

The integral in the denominator of (23) is bounded above and below as follows:

$$\frac{1-\hat{c}}{\chi} < \int_0^{(1-\hat{c})/\chi} \exp\{\alpha_1\eta(\hat{c}+\chi\eta/2)\}d\eta < \frac{1-\hat{c}}{\chi}e^{\theta}.$$

Substituting with the above expressions then yields

$$n_{2L}(0,x^*/\chi) < n_2(0,x^*/\chi) < n_{2U}(0,x^*/\chi),$$

where

$$n_{2L}(0,x^*/\chi) = \frac{e^{\theta}}{1+\frac{\beta x^*}{\gamma}+\frac{\beta(1-\hat{c})}{\gamma}(e^{\theta}-1)},$$

$$n_{2U}(0,x^*/\chi) = \frac{e^{\theta}}{1+\frac{\beta x^*}{\gamma}}.$$

We deduce that angiogenesis fails if $n_{2U}(0,x^*/\chi) < 1$, which, on rearrangement, yields the inequality

$$e^{\theta} = \exp\{\frac{\alpha_1}{2\chi}(1-\hat{c}^2)\} < 1+\frac{\beta x^*}{\gamma}.$$

Imposing $n_{2L}(0,x^*/\chi) > 1$ defines a second region of parameter space in which successful angiogenesis is predicted. For example, fixing $\beta/\gamma = 0.5, \hat{c} = 0.2, \chi = 0.4$ and $x^* = 0.9$ and rearranging these inequalities, it is possible to predict ranges of α_1 for which angiogenesis succeeds ($\alpha_1 > 0.47$) and fails ($\alpha_1 < 0.31$). In figures 5 and 6 capillary tip density profiles, obtained using the simplified model (with $\alpha_0 = 0$), are plotted. In both figures we fix $\beta/\gamma = 0.5, \hat{c} = 0.2, \chi = 0.4$ and $x^* = 0.9$. As anticipated from the theoretical bounds on α_1, with $\alpha_1 = 0.7$ in figure 5 successful angiogenesis is observed, whereas with $\alpha_1 = 0.3$ in figure 6 angiogenesis fails.

In conclusion, the success or failure of angiogenesis is essentially governed by the balance between the proliferating parameter grouping α_1/χ and the 'death' parameters $\hat{c}, x^*$ and β/γ. For example, the parameter $\hat{c}$ denotes the threshold TAF concentration at which (secondary) tip proliferation is initiated. Given the steady TAF profile adopted here, increasing $\hat{c}$ reduces the size of the domain in which tip proliferation occurs, making angiogenesis less likely to occur. Increasing x^* has a similar effect whilst the appearance of the ratio α_1/χ may be explained thus. The larger the speed of the vascular front χ, the less time is available for tip proliferation before the front reaches the tumour. Thus, to ensure vascularisation occurs the tip proliferation rate α_1 must increase at least as quickly as χ. The effect that increasing the parameter grouping β/γ has on diminishing the success of angiogenesis follows analogously.

5 Conclusions

In this paper we have adapted and extended Balding and McElwain's continuum model of capillary growth in an attempt to reproduce more accurately the salient features of tumour angiogenesis. By posing the model on a finite, rather than a semi-infinite, domain, we believe we are able to provide a more realistic approximation of the physical environment and also to simulate a range of experimental configurations, for example, varying the tumour-limbus separation distance. The inclusion of TAF consumption terms in the reaction-diffusion equation governing c, and of a secondary tip proliferation rate, triggered by a threshold TAF concentration distinguishes our model from Balding and McElwain's. The prescription at the limbus of a tip density which decays to zero is another novel feature of our model, and is an attempt to describe the experimental observation that, after the initial formation of capillary buds at the limbus, sprout tips no longer originate from there.

The main weakness of the continuum model presented here is its inability to distinguish between anastomosis and tip death - a reduction in tip density may be ascribed to either effect. This is because angiogenesis is essentially a two-dimensional process, with tips sprouting in directions other than that of the propagating front. Improvements to the model which we envisage making are, therefore, an extension to two space dimensions and distinction between cell-death and anastomosis. In addition, thickening of the branches and other changes to the vascular network which are direct consequences of anastomosis should be included. We believe that our assumption that chemotaxis dominates random motility and our choice of 10^{-3} for the parameter μ are appropriate for this particular model. However, we note that this estimate does not agree with estimates for the random motility coefficients for endothelial cells as found by Rupnick *et al.* (1990), Stokes *et al.* (1990, 1991). Justifications for this apparent discrepancy were given at the end of section 2.

Inspite of the above shortcomings, the numerical simulations show that our model is, in fact, able to reproduce many of the qualitative features of tumour angiogenesis, some not observed in earlier models. Firstly, depending on the balance between tip proliferation, tip decay and the strength of the chemotactic field, successful neovascularization of the tumour or failure of the tumour to secure a vascular network may result (see figures 1 to 3). When successful neovascularization occurs, the advancing front exhibits the brush-border effect observed by Muthukkaruppan *et al.* (1982), with an increasingly developed vascular network evolving behind the leading tip front, and the resolution of these two profiles a direct consequence of secondary tip proliferation. Further, the speed of the front increases as the tumour is approached, a result consistent with experimental measurements by Folkman (1986).

The numerical results suggest that the TAF concentration rapidly relaxes to a steady profile which is monotonically decreasing in space. This fact coupled with the estimates of $\mu \sim 10^{-3}$ in equations (8), (9), lead to the development of a caricature model which provides insight into how the balance between chemotaxis, tip proliferation and tip death affect the ability of the tumour to induce a vascular response from the limbus. Using the method of characteristics to analyse the resulting one-dimensional hyperbolic equation for the tip density, it is possible to demonstrate that the simplified model possesses several of the properties of the original model, mentioned above. Firstly, we were able to verify that the tip density profile propagates towards the tumour as a wave with increasing speed. Secondly, we showed that the tip density front precedes the vessel density front. In addition, we were able to define the success and failure of angiogenesis in terms of known parameters. For example, increasing the ratio of the rate of tip-to-branch anastomosis to the rate of branch decay (β/γ) reduces the likelihood of successful angiogenesis, whilst increasing the parameter grouping α_1/χ has the reverse effect.

References

[1] Adam, J.A. and S. Maggelakis. 1990. Diffusion regulated growth characteristics of a spherical prevascular carcinoma. *Bull. Math. Biol.* **52**, 549-582.

[2] Ausprunk, D.H. and J. Folkman. 1977. Migration and proliferation of endothelial cells in preformed and newly formed blood vessels during tumour angiogenesis. *Microvasc. Res.* **14**, 53-65.

[3] Ausprunk, D.H., D.R. Knighton, and J. Folkman. 1974. Differentiation of vascular endothelium in the chick chorioallantois: A structural and autoradiographic study. *Dev. Biol.* **38**, 237.

[4] Balding, D. and D.L.S, McElwain. 1985. A mathematical model of tumour-induced capillary growth. *J. Theor. Biol.* **114**, 53-73.

[5] Berestycki, H., B. Nicolaenko and B. Scheurer. 1983. Travelling wave solutions to reaction-diffusion systems modelling combustion. *Contemporary Mathematics. American Mathematical Society.* **17**, 189-207.

[6] Birdwell, C.R., G.L. Gospadorowicz, and G.L. Nicholson, 1977. Factors from 3T3 cells stimulate proliferation of cultured vascular endothelial cells. *Nature (London)* **268**, 528-531.

[7] Chaplain, M.A.J. 1990. Mathematical models for the growth of solid tumours and the tip morphogenesis of *Acetabularia*. Ph.D. Thesis, University of Dundee.

[8] Chaplain, M.A.J. and A.M. Stuart. 1991. A mathematical model for the diffusion of tumour angiogenesis factor into the surrounding host tissue. *IMA J. Math. Appl. Med. Biol.* **8**, 191-220.

[9] Chaplain, M.A.J. and A.M. Stuart. 1993. A model mechanism for the chemotactic response of endothelial cells to tumour angiogenesis factor. *I.M.A. J. Math. Appl. Med. Biol.* **10**, 149-168.

[10] Deshpande, R.G. and Y.I. Shetna. 1989. Isolation and characterisation of tumour angiogenesis factor from solid tumours and body fluids from cancer patients. *Indian J. Med. Res.* **90**, 241-247.

[11] Eddy, H.A. and G.W. Casarett, 1973. Development of the vascular system in the hamster malignant neurolemmoma. *Microvasc. Res.* **6**, 63-82.

[12] Edelstein, L. 1982. The propagation of fungal colonies: A model for tissue growth. *J. Theor. Biol.* **98**, 679-701.

[13] Erroi, A.L., P.M. Kumar and S. Kumar. 1986. Effects of a purified low molecular weight tumour angiogenesis factor on cell morphology of bovine brain capillary endothelial cells growing on native collagen substratum. *Anticancer Res.* **6**, 1045-1051.

[14] Fife, P.C. 1979. Mathematical aspects of reacting and diffusing systems. *Lecture notes in biomathematics.* **28**. Springer-Verlag, Berlin.

[15] Folkman, J. 1974. Tumor angiogenesis. *Adv. Cancer Res.* **19**, 331-358.

[16] Folkman, J. 1976. The vascularisation of tumours. *Sci. Am.* **234**, 58-73.

[17] Folkman, J. 1986. The vascularization of tumours. In *Cancer biology: readings from Scientific American*, (Ed. Friedberg, E.C.) 115-124.

[18] Folkman, J. and M. Klagsbrun. 1987. Angiogenic factors. *Science* **235**, 442-447.

[19] Gimbrone, M.A., R.S. Cotran, S.B. Leapman and J. Folkman. 1974. Tumour growth and neovascularization: An experimental model using the rabbit cornea. *J. Natl. Cancer Inst.* **52**, 413-427.

[20] Gross, J., R.G. Azizkhan, C. Biswas, R.R. Bruns, D.S.T. Hseih and J. Folkman. 1981. Inhibition of tumour growth, vascularisation and collagenolysis in the rabbit cornea by medroxyprogesterone. *Proc. Natl. Acad. Sci. USA* **78**, 1176-1180.

[21] Ishiwata, I., C. Ishiwata, M. Soma, I. Ono, T. Nakaguchi, and H. Ishikawa, 1988. Tumour angiogenic activity of gynecologic tumour cell lines on the chorioallantoic membrane. *Gynecol. Oncol.* **29**, 87-93.

[22] Jaffe, A.E., R.L. Nachman, C.G. Becker and C.R. Minick 1973. Culture of human endothelial cell lines derived from umbilical veins. *J. Clin. Invest.* **52**, 2745.

[23] Klagsbrun, M., D.R. Knighton, and J. Folkman. 1976. Tumour angiogenesis activity in cells grown in tissue culture. *Cancer Res.* **36**, 110-114.

[24] Kumar, P., A. Erroi, A. Sattar and S. Kumar. 1985. Weibel-Palade bodies as a marker for neovascularization induced by tumour and rheumatoid angiogenesis factors. *Cancer Res..* **45**, 4339-4348.

[25] Langer, R., H. Conn, J. Vacanti, C. Haudenschild and J. Folkman. 1980. Control of tumour growth in animals by diffusion of an antiogenesis inhibitor. *Proc. Natl. Acad. Sci. USA* **77**, 4331-4335.

[26] Madri, J.A. and B.M. Pratt 1986. Endothelial cell-matrix interactions: *In vitro* models of angiogenesis. *J. Histochem. Cytochem.* **34**, 85.

[27] Muthukkaruppan, V.R., L. Kubai and R. Auerbach. 1982. Tumour-induced neovascularization in the mouse eye. *J. Natl. Cancer Inst.* **69**, 699-705.

[28] Paku, S. and N. Paweletz. 1991. First steps of tumor-related angiogenesis. *Lab. Invest.* **65**, 334-346.

[29] Paweletz, N. and M. Knierim. 1989. Tumour-related angiogenesis. *Critical Reviews in Oncology/Hematology* **9**, 197-242.

[30] Rupnick, M.A., Stokes, C.L., Williams, S.K. and D.A. Lauffenburger. 1988. Quantitative analysis of human microvessel endothelial cells using a linear under-agarose assay. *Lab. Invest.* **59**, 363-372.

[31] Stokes, C.L., Rupnick, M.A., Williams, S.K. and D.A. Lauffenburger. 1990. Chemotaxis of human microvessel endothelial cells in response to acidic fibroblast growth factor. *Lab. Invest.* **63**, 657-668.

[32] Stokes, C.L. and D.A. Lauffenburger. 1991. Analysis of the roles of microvessel endothelial cell random motility and chemotaxis in angiogenesis. *J. Theor. Biol.* **152**, 377-403.

[33] Stokes, C.L., D.A. Lauffenburger and S.K. Williams. 1991. Migration of individual microvessel endothelial cells: stochastic model and parameter measurement. *J. Cell Science.* **99**, 419-430.

[34] Strydom, D.J., J.W. Fett, L.R. Lobb, E.M. Alderman, J.L Bethune, J.F. Riordan and B.L. Vallee. 1985. Amino acid sequence of human tumour derived angiogenin. *Biochemistry* **24**, 5486-5494.

[35] Williams, W. 1980. *Partial differential equations.* Oxford University Press.

[36] Willmott, N., J. Goldberg, R. Bessent, J. McKillop and C. McArdle. 1991. Abnormal vasculature of solid tumours: Significance for microsphere-based targetting strategies. *Int. J. Radiat. Biol.* **60**, 195-199.

Figure Legends

Figure 1(a): Profile of the capillary tip density propagating from the limbus at $x = 1$ through the external host tissue to the tumour implant at $x = 0$. Secondary tip proliferation is included. Profiles are plotted at times $t = 0.2, 0.4, ..., 1.6$. Parameter values: $\alpha_0 = 50, \alpha_1 = 10, \beta = 50, \gamma = 0.25, \chi = 0.4, \lambda = 1, \hat{c} = 0.2$.

Figure 1(b): Profile of the vessel density during successful angiogenesis, with parameter values as per figure 1(a).

Figure 1(c): Profile of the TAF concentration during successful angiogenesis, with parameter values as per figure 1(a).

Figure 2(a): Profile of the capillary tip density showing unsuccessful angiogenesis, brought about by a reduction in the strength of the underlying TAF field. All parameter values are the same as in figure 1, except for increases in the rate of TAF decay (λ) and the threshhold TAF concentration ($\hat{c}$) which marks the onset of secondary tip proliferation. Profiles are plotted at times $t = 0.2, 0.4, ..., 2.0$. Parameter values: $\alpha_0 = 50, \alpha_1 = 10, \beta = 50, \gamma = 0.25, \chi = 0.4, \lambda = 10, \hat{c} = 0.5$.

Figure 2(b): Profile of the vessel density, with parameter values as per figure 2(a).

Figure 2(c): Profile of the TAF concentration during failed angiogenesis, with parameter values as per figure 2(a).

Figure 3(a): Profile of the capillary tip density showing successful angiogenesis with no secondary tip proliferation. Profiles are plotted at times $t = 0.2, 0.4, ..., 2.0$. Parameter values: $\alpha_0 = 50, \alpha_1 = 0, \beta = 50, \gamma = 0.25, \chi = 0.4, \lambda = 10, \hat{c} = 0.5$.

Figure 3(b): Profile of the vessel density during successful angiogenesis, with no secondary tip proliferation and parameter values as per figure 3(a).

Figure 3(c): Profile of the TAF concentration during successful angiogenesis, with no secondary tip proliferation and parameter values as per figure 3(a).

Figure 4: Characteristic diagram for the simplified model.

Figure 5: Solution of the simplified model showing the evolution of the capillary tip density during successful angiogenesis. Profiles are plotted at times $t = 0.0, 0.2, 0.4, ..., 2.2$. Parameter values: $\alpha_1 = 0.7, \beta/\gamma = 0.5, \chi = 0.4, \hat{c} = 0.2, x^* = 0.9$.

Figure 6: Solution of the simplified model showing the evolution of the capillary tip density during unsuccessful angiogenesis, brought about by a reduction in the rate of secondary tip proliferation. All parameter values are the same as in figure 5, except for a reduction in the rate of secondary tip proliferation (α_1). Profiles are plotted at times $t = 0.0, 0.2, 0.4, ..., 2.2$. Parameter values: $\alpha_1 = 0.3, \beta/\gamma = 0.5, \chi = 0.4, \hat{c} = 0.2, x^* = 0.9$.

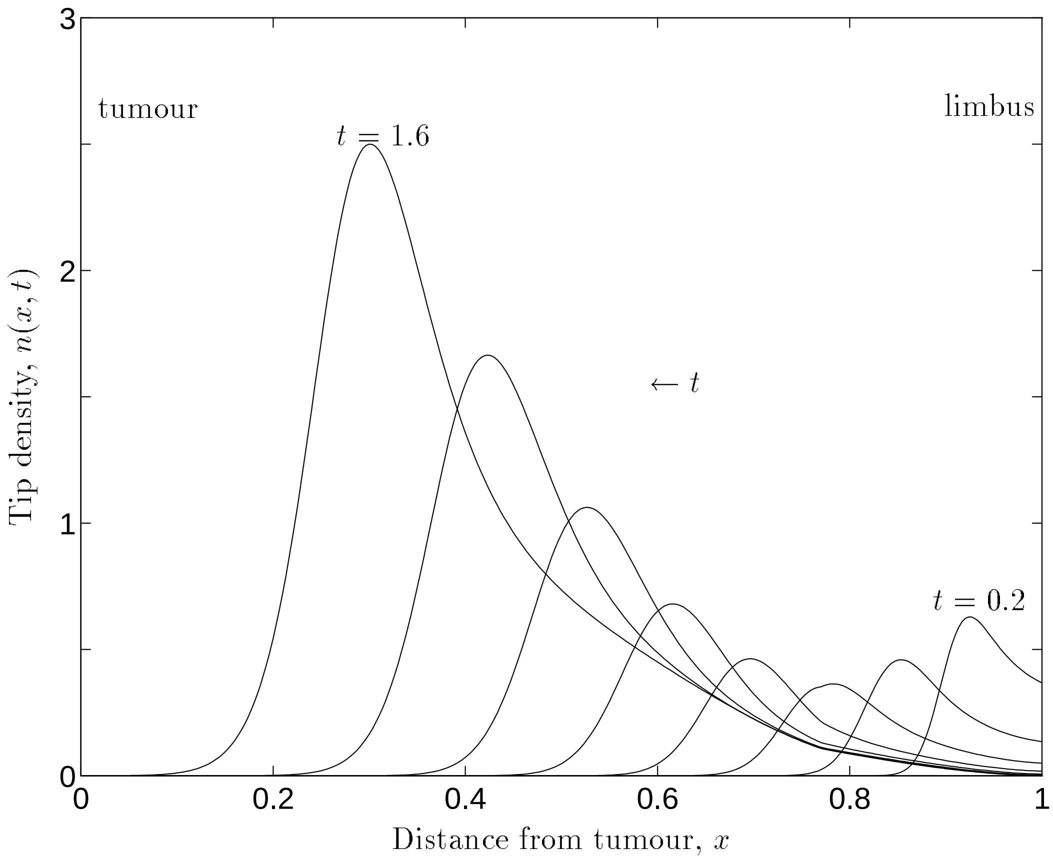

Byrne & Chaplain: Figure 1(a)

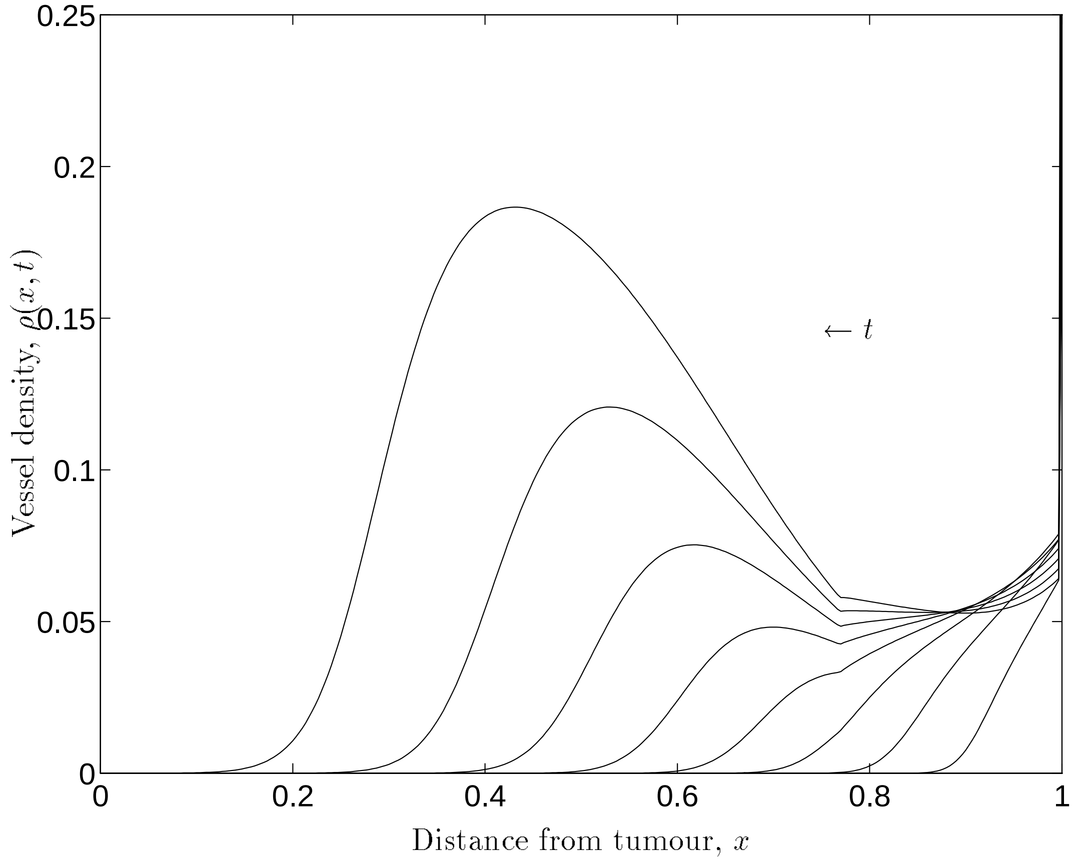

Byrne & Chaplain: Figure 1(b)

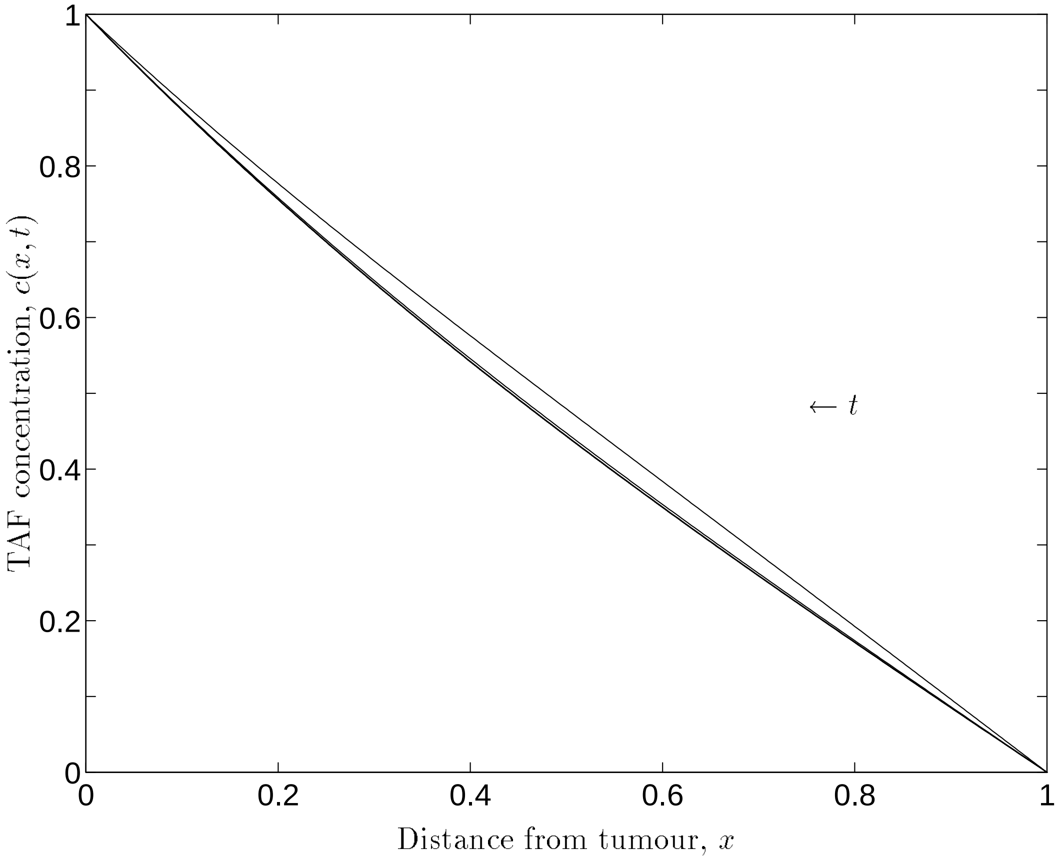

Byrne & Chaplain: Figure 1(c)

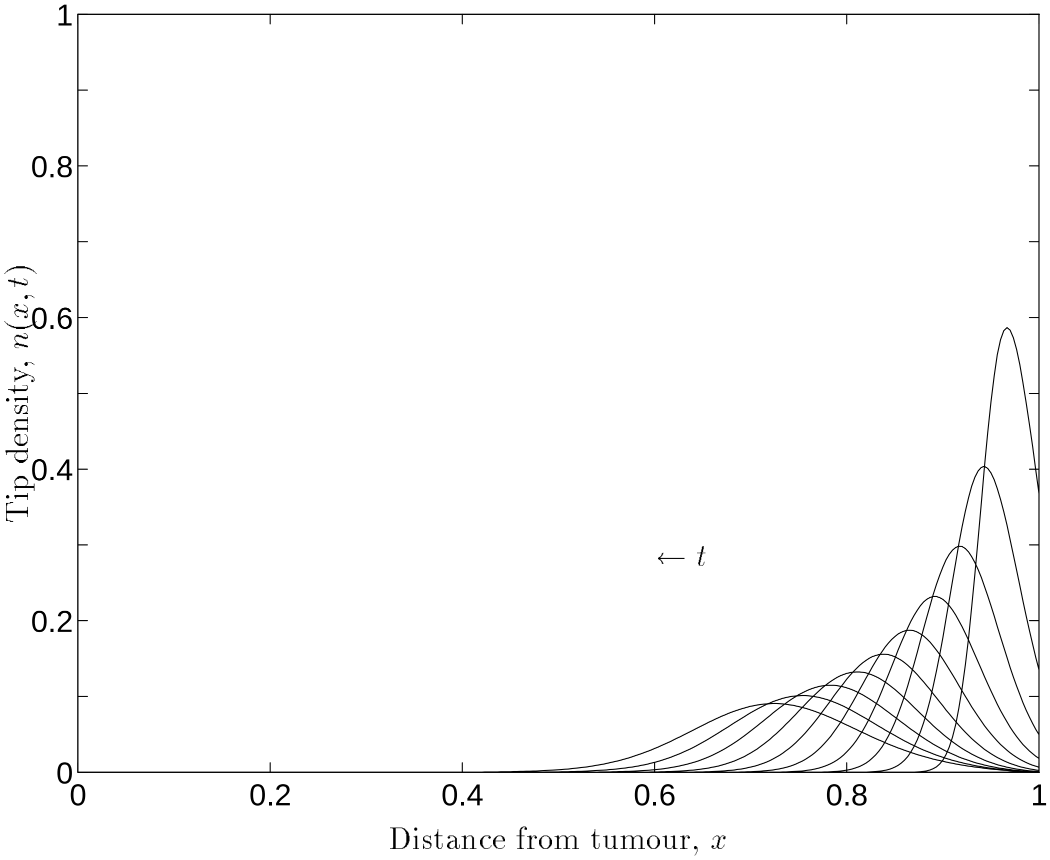

Byrne & Chaplain: Figure 2(a)

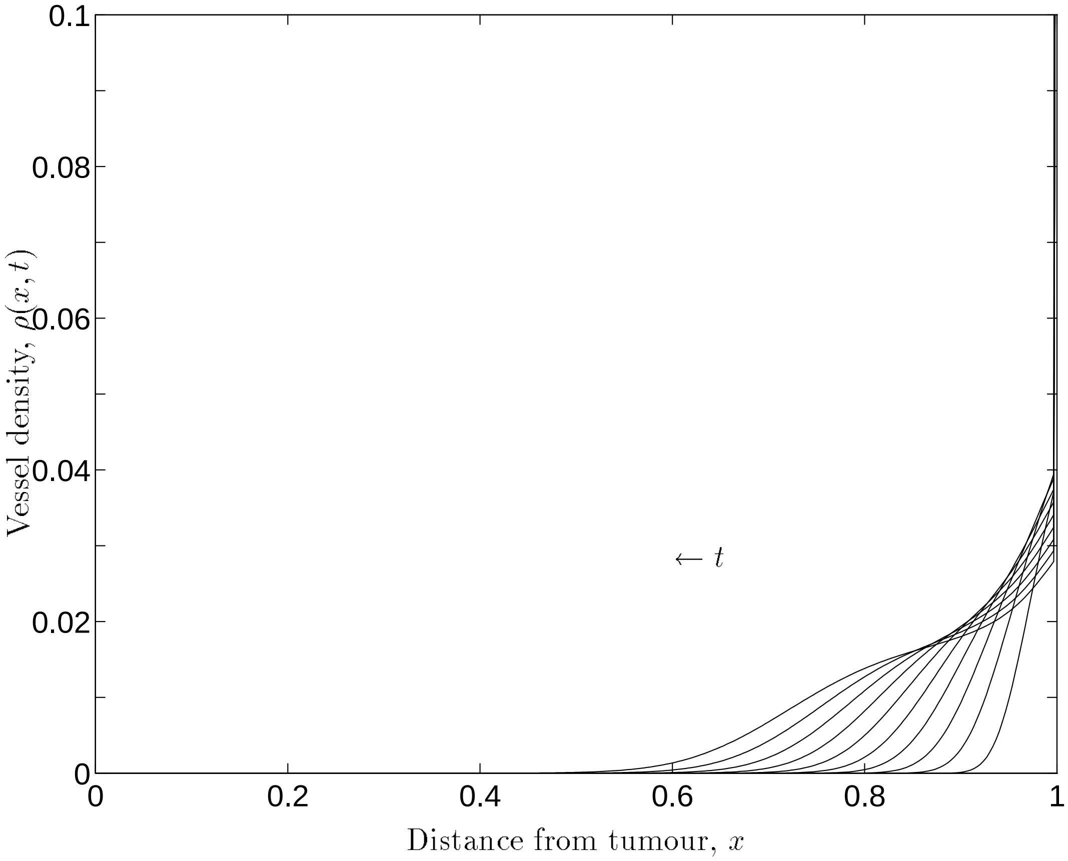

Byrne & Chaplain: Figure 2(b)

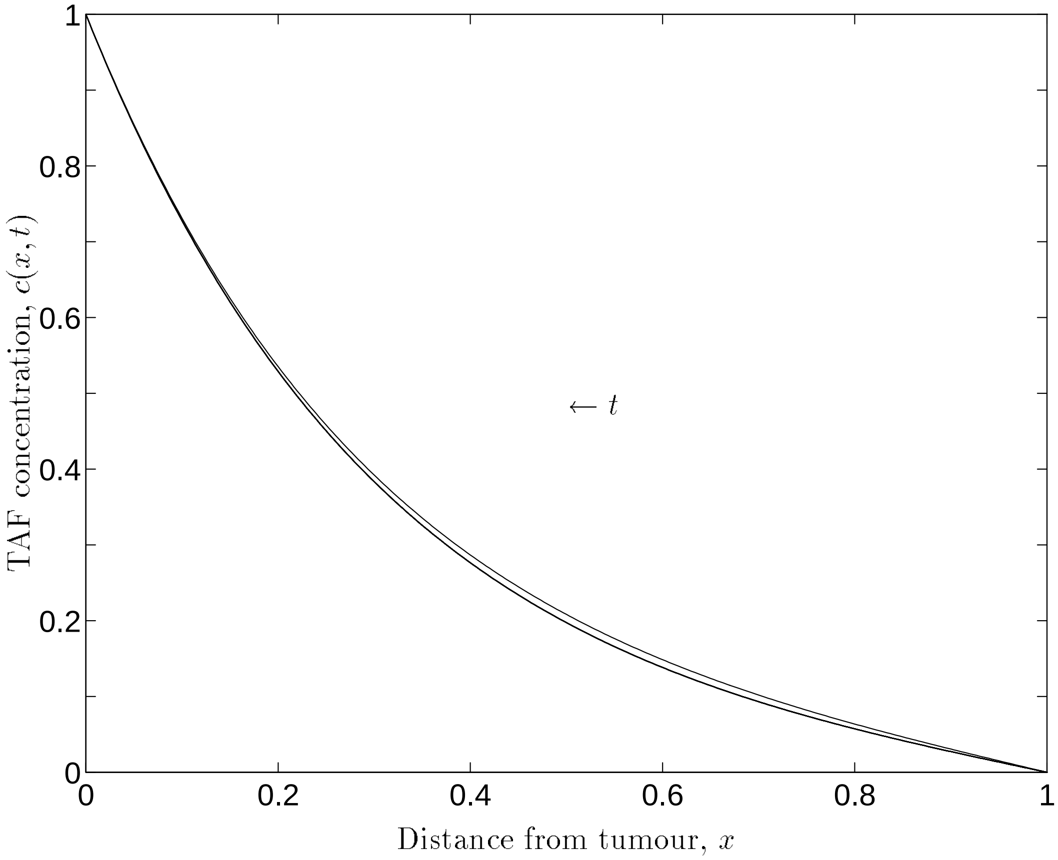

Byrne & Chaplain: Figure 2(c)

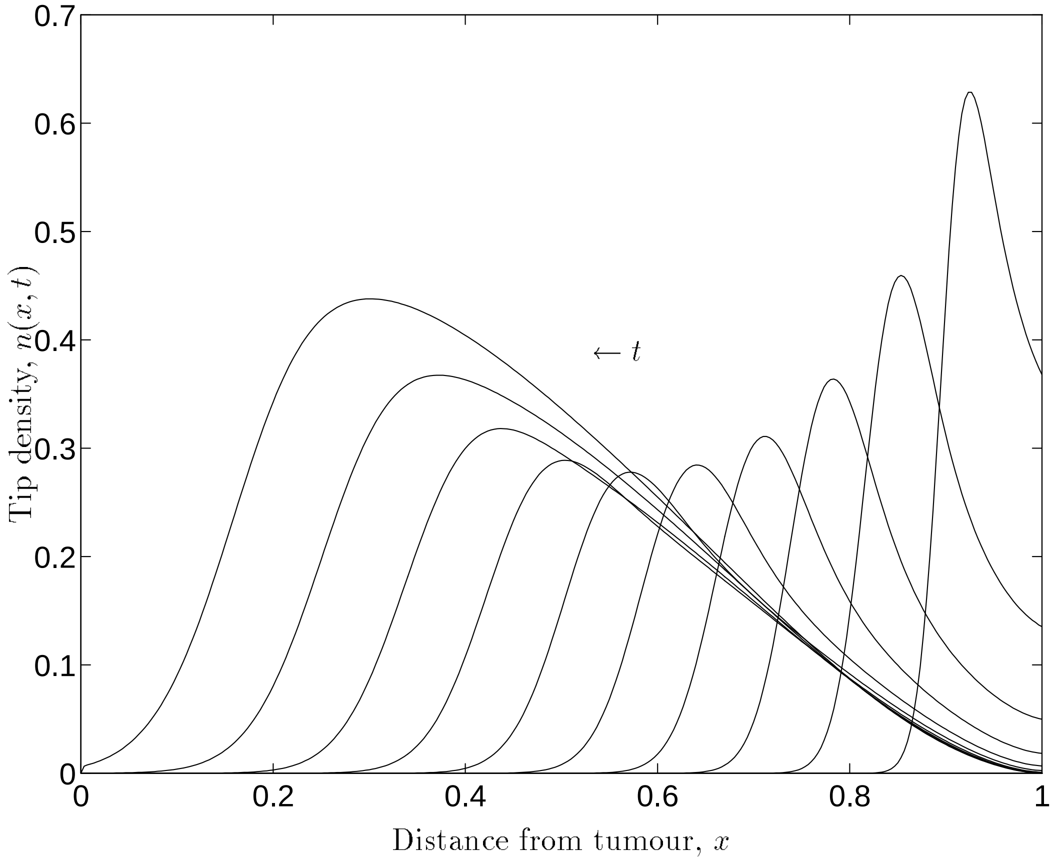

Byrne & Chaplain: Figure 3(a)

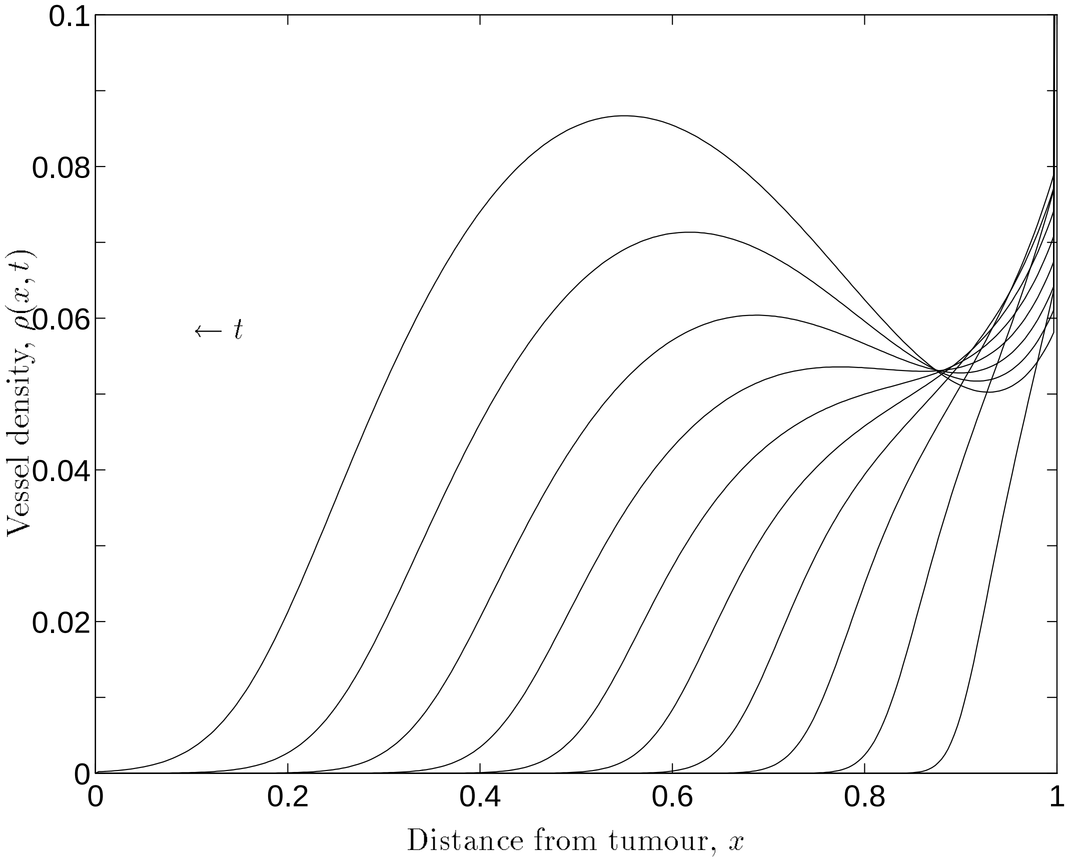

Byrne & Chaplain: Figure 3(b)

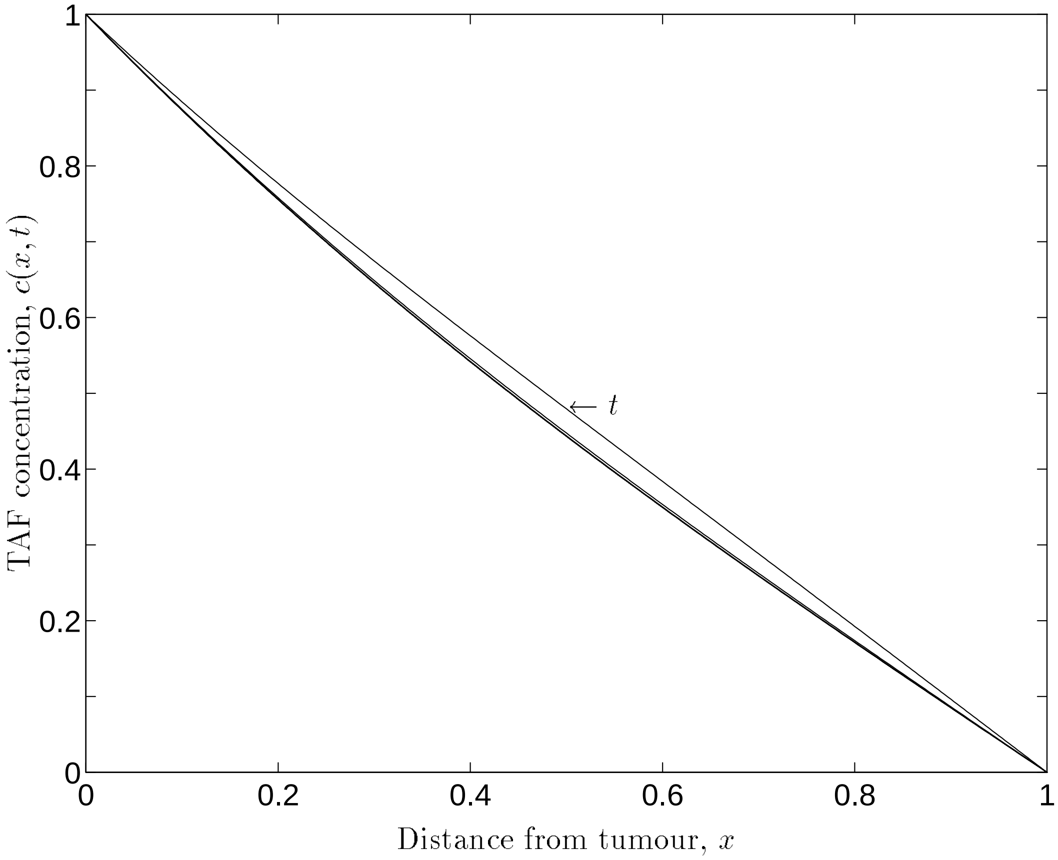

Byrne & Chaplain: Figure 3(c)

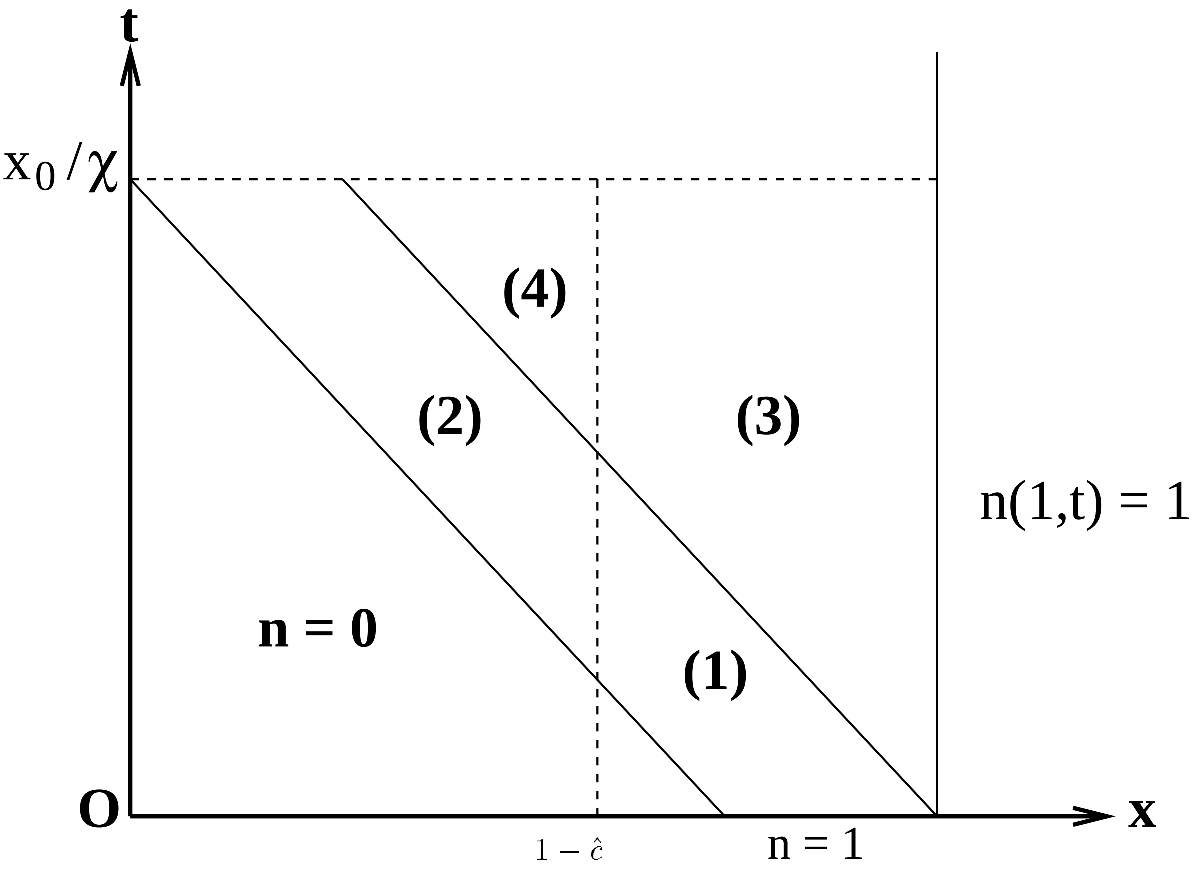

Byrne & Chaplain: Figure 4

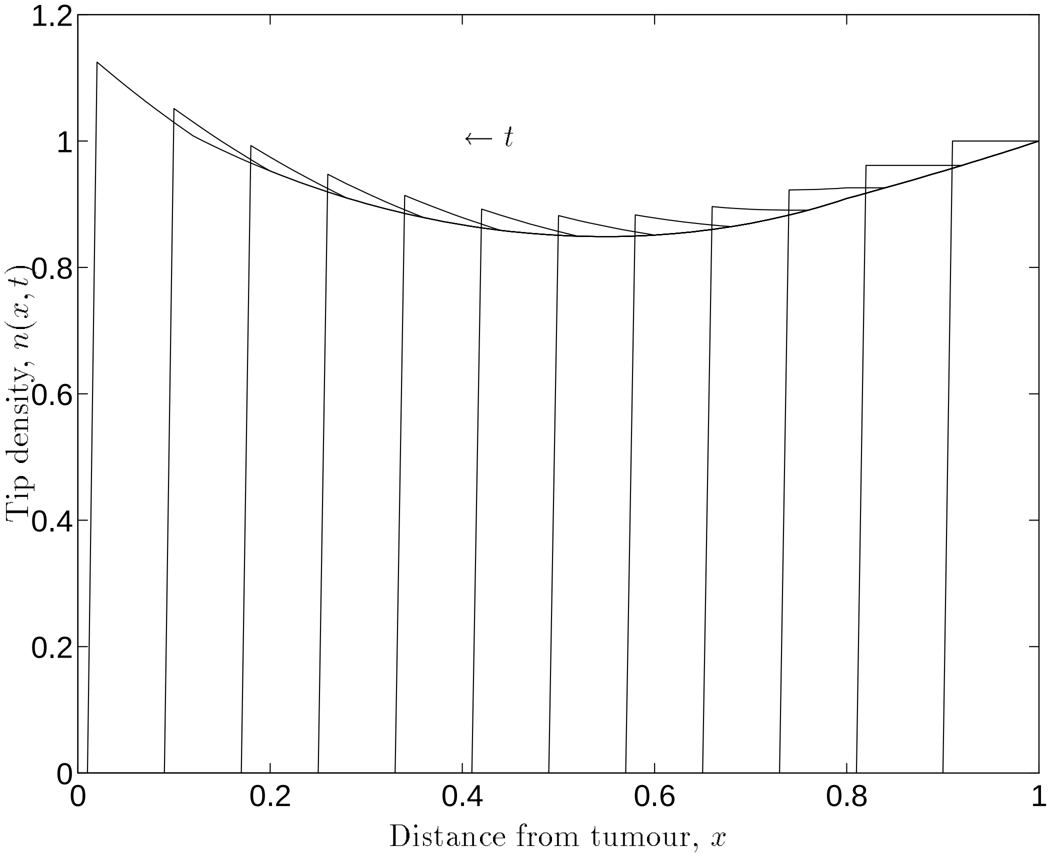

Byrne & Chaplain: Figure 5

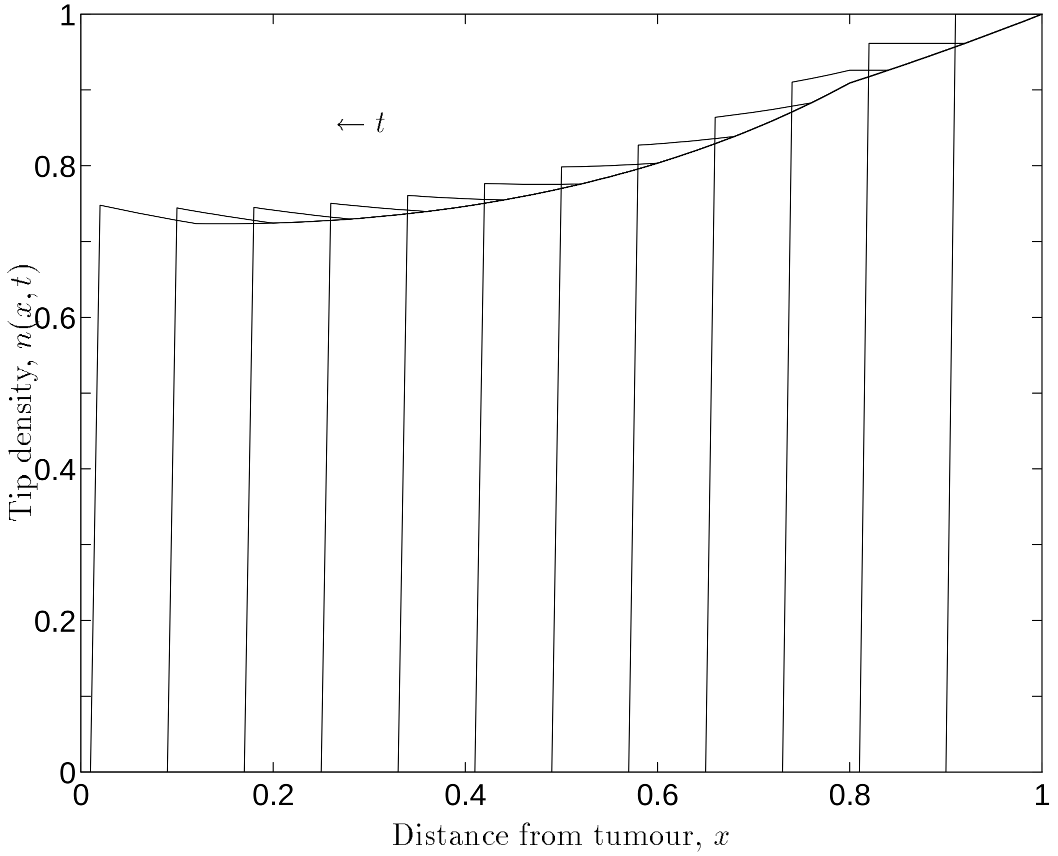

Byrne & Chaplain: Figure 6